JOURNAL OF PROPULSION AND POWER
Vol. 26, No. 4, July–August 2010

Numerical Simulation of Supersonic Nonpremixed Turbulent Combustion in a Scramjet Combustor Model

Arnaud Mura* and Jean-François Izard
Ecole Nationale Supérieure de Mécanique et d'Aérotechnique, 86961 Futuroscope, France

DOI: 10.2514/1.48074

Nonpremixed turbulent combustion is studied in situations relevant to those encountered in advanced airbreathing engines operating at high flight Mach number values. Accurate simulations would require modeling both finite rate chemical kinetics and molecular diffusion effects (mixing) as well as the complex compressible flowfield structure associated with the presence of multiple shock and expansion waves that significantly influence combustion. The chemical kinetics are modeled by using a Lagrangian framework for turbulent combustion that has been recently extended to reactive high-speed flows. The corresponding framework incorporates both finite rate kinetics and turbulent molecular mixing rates with minimal additional parameters. An efficient anisotropic mesh adaptation strategy is used to obtain a satisfactory description of both nonreactive and reactive compressible flowfields. The present study confirmed that the proposed approach provides a well-suited framework for future developments devoted to nonpremixed turbulent combustion modeling in high-speed flows. A detailed comparison with data gathered from an experimental study of a laboratory scramjet model indicated the validity of the approach.

Nomenclature

D	=	molecular diffusivity
$\boldsymbol{\mathcal{D}}$	=	diffusive flux vector
Da	=	Damköhler number
$\mathcal{D}_{(\xi,Y)}$	=	domain of definition of the joint scalar probability density function
E	=	energy
$\boldsymbol{\mathcal{F}}$	=	convective flux vector
h	=	enthalpy
k	=	turbulent kinetic energy
Ma	=	Mach number
Mt	=	turbulent Mach number
$\tilde{P}(Y)$	=	marginal probability density function of oxygen mass fraction Y
$\tilde{P}(\xi)$	=	marginal probability density function of mixture fraction ξ
$\tilde{P}(\xi, Y)$	=	joint probability density function of mixture fraction ξ and oxygen mass fraction Y
p	=	pressure
$\bar{q}$	=	Reynolds average of quantity q
$\widetilde{q}$	=	Favre average of quantity q
$\boldsymbol{\mathcal{S}}$	=	source term vector
Sc	=	Schmidt number
T	=	temperature
t	=	time
u	=	velocity
$\boldsymbol{\mathcal{U}}$	=	solution vector (conservative variables)
$\boldsymbol{x}$	=	Cartesian coordinates
Y	=	oxygen mass fraction
ϵ	=	turbulent energy dissipation rate
ν	=	kinematic viscosity
ξ	=	mixture fraction
ρ	=	density
τ	=	mixing time scale
ϕ	=	test function (finite volume formulation)
χ	=	scalar dissipation rate
ψ	=	test function (finite element formulation)
ω_Y	=	chemical production rate of Y

Subscripts

k	=	component k
st	=	stoichiometric
t	=	total (for instance, h_t is the total enthalpy)
T	=	turbulent

Superscripts

$'$	=	fluctuations with respect to Reynolds average
$''$	=	fluctuations with respect to Favre average

I. Introduction

DESPITE the promising progress made toward the use of alternative flight solutions such as, among others, the pulsed detonation technology, high-speed airbreathing engines remain the propulsion system of choice, and both ramjet and scramjet strategies still represent the most attractive solutions for supersonic ($1 < Ma < 5$) and hypersonic ($5 < Ma < 15$) regimes, respectively. In the classical ramjet technology, the air inlet flow is progressively decreased to reach subsonic velocities, thus favoring the stabilization of the nonpremixed flame within the combustion chamber [1]. However, for very high values of the flight Mach number Ma, this deceleration takes place through successive oblique shock waves and the resulting conversion of kinetic energy into thermal energy leads to extremely high temperature levels at which combustion heat release is dramatically reduced. This behavior is associated with losses of total pressure and a corresponding loss of thrust. With the objective to minimize the influences of both the high-temperature dissociation processes and the net loss of thrust that are induced by the strong deceleration that takes place in ramjets, attention has been focused on the possibility of performing combustion at supersonic speeds, thus leading to the concept of scramjet (supersonic combustion ramjet) engines [2].

In the scramjet technology, the airflow through the whole engine (including the combustion chamber) remains supersonic. The considered fuel is generally hydrogen and scramjets operate through a mixing-controlled supersonic combustion of fuel within a stream of compressed air scooped from the atmosphere. The values of the specific impulse obtained within a scramjet can theoretically be

Received 10 November 2009; revision received 1 April 2010; accepted for publication 1 April 2010.

*Institut P′, UPR 3346 du CNRS, CNRS–ENSMA–Université de Poitiers, Département Fluide, Thermique et Combustion, ENSMA, Téléport 2, 1 Avenue Clément Ader, B.P. 40109, 86961 Futuroscope Chasseneuil Cedex France; arnaud.mura@ensma.fr (Corresponding Author).

higher than those obtained with rocket engines [3,4], but its restricted operating range requires it to be combined with another engine (dual-mode scramjet) [1]. Scramjet technology development remains very challenging because only limited run time investigations can be performed in ground test facilities and full-scale testing requires flight speeds above Mach 8. Thus, the representation of the corresponding reactive flowfields still represents a tremendous challenge for computational studies and several specific modeling difficulties arise. Among the different issues that must be addressed in this field, we can mention the following ones: the efficiency of the combustor is strongly related to the stability and completion of combustion within the engine length [3–5]. The achievement of the combustion process is determined by the level of mixing between the reactants, which has been found to be crucially influenced by high Mach number effects. Special attention has been paid very early to these fundamental issues. For instance, it has been evidenced that the large-scale nonreactive mixing growth rate in supersonic mixing layers is tremendously affected by compressibility effects [6,7]. The influence of incident shock waves on both mixing efficiency and flame stability has been also investigated [8,9]. Indeed, within a supersonic combustion chamber the question of the flame-holding is seriously complicated by successive interactions of shock waves with the flame front. Among others, Fujimori et al. [8] have analyzed the possibility of taking benefit from the shock waves development to make it easier to stabilize combustion downstream of an injector strut. Their experimental results have showed that the interaction of shock waves with subsonic flow regions can modify the flowfield sufficiently to favor the flame stabilization processes. In addition, the description of the nonpremixed combustion in such high-velocity reactive flows is clearly influenced by compressibility effects, shock waves, turbulent mixing, and chemical kinetics processes [4,5,9,10].

In this framework, the essential aims of the present study are as follows:

1) Apply a closure based on the use of the MIL (modèle intermittent Lagrangian) [11,12] model that has been recently extended to deal with some specific features of nonpremixed turbulent combustion in supersonic flows [13,14].

2) Use this closure conjointly with an efficient mesh adaptation strategy that is able to render the complexity of the compressible flowfield with a sufficient degree of confidence.

3) Assess the relevance of the computational model proposed to simulate turbulent combustion in high-speed flows with a detailed comparison of numerical results with a well-documented experimental database.

In [14], the modeling proposal retained here has been previously applied with success to simulate the experiments conducted by Cheng et al. [15]. The corresponding experimental setup, which consists of two high-speed coflowing jets of hydrogen and vitiated air discharging into the atmosphere, is considered as a classical preliminary validation step in the field of supersonic combustion [16–18]. For the purpose of the present study, the computational model is used in conjunction with an anisotropic mesh adaptation (AMA) strategy; this now allows considering fully compressible flowfields, featuring successive shock and expansion waves, that are more representative of those encountered in real scramjet engines. To validate the computational model in such conditions, we retain the laboratory scramjet model investigated by Waidmann et al. [19,20]. In the corresponding experimental setup, hydrogen is injected from the base of a wedge-shaped strut injector at sonic conditions into a stream of vitiated air at a Mach number $Ma = 2$. Previous computational studies of this laboratory scramjet engine include both recent LES (large eddy simulation) and RANS (Reynolds-averaged Navier–Stokes) simulations [21–25]. Needless to say, the characterization of the unsteady features in such compressible turbulent reactive high-speed flows still remains a difficult task, from both experimental and numerical points of view, and so the evaluation of numerical models capabilities remains essentially performed through the comparisons of steady-state solutions with the corresponding experimental data that gather statistical informations about the flowfield. In this respect, the RANS strategy provides the most suitable framework to obtain such steady-state solutions for flows at high Reynolds number, especially for design and optimization purposes. In turbulent nonpremixed flames, the competition between molecular diffusion effects (namely, micromixing or scalar dissipation) and chemical kinetics must be taken into account. The Lagrangian framework retained in the present work is able to represent such effects in supersonic turbulent reactive flows [14] and one of the main objectives of the study is to confirm the ability of the corresponding computational model to predict turbulent combustion in high-speed confined flows featuring significant pressure discontinuities.

The present manuscript is organized as follows: the essential features of the MIL model are first briefly recalled in the next section while the computational strategy and modeling are presented in a third section. The experimental test case is then briefly described, and the corresponding numerical results are then presented and discussed.

II. Lagrangian Intermittent Framework for High-Speed Turbulent Nonpremixed Combustion

The turbulent combustion modeling framework retained in the present study is based on the early proposal of Borghi and Pourbaix [11] and Borghi and Gonzalez [12]. The MIL model aims at representing the competition that exists between micromixing phenomena and finite rate chemistry effects in nonpremixed flames. Consideration of such finite rate chemistry effects requires the use of at least two scalar variables: one to represent the variations of composition in the unburned mixture (mixture fraction ξ) and the other to follow the departures from chemical equilibrium. For the latter there exists at least two distinct possibilities. The first relies on the consideration of the scalar dissipation rate of the mixture fraction variable [i.e., $\chi_\xi = D(\partial\xi/\partial x_\alpha)^2$] or, eventually, its value for stoichiometric conditions $\chi_{\xi_{st}}$, as it is usually envisaged in cases in which local flamelets are assumed to be thin enough and locally one-dimensional: i.e., for sufficiently moderate levels of strain rate and curvature [26]. The second possibility is more general and introduces a so-called progress variable Y that characterizes the progress of chemical reactions within the domain of definition $\mathcal{D}_{(\xi,Y)}$ for the couples (ξ, Y). This domain of definition $\mathcal{D}_{(\xi,Y)}$, which is also denoted as composition space in the following, is bounded by the pure mixing line $Y = Y_{Da\to 0}(\xi)$ and the chemical equilibrium $Y = Y_{Da\to\infty}(\xi)$. In the previous expressions, Da denotes a Damköhler number based on the ratio of two characteristic time scales: a mechanical one (representative of the flowfield dynamics) and a chemical one.

As turbulent reactive flows are considered, and since the behavior of combustion chemistry is highly nonlinear [27], the joint probability density function (PDF) of the two scalar quantities is needed to render the influence of composition fluctuations. The framework retained for the purpose of the present study relies on presumed PDF shapes [28]. In comparison with the transported PDF approach [18,29], the main attractive feature of such frameworks relies on their robustness and their significantly lower computational costs which makes them very efficient for both RANS and LES simulations of engineering turbulent reactive flows. When the scalar dissipation rate χ_ξ is retained as a characteristic variable to describe the departures from chemical equilibrium, the dynamics of each scalar are usually considered to be statistically independent [i.e., $\tilde{P}(\xi, \chi_\xi) = \tilde{P}(\xi)\tilde{P}(\chi_\xi)$], and the problem is reduced to the determination of the two marginal PDF $\tilde{P}(\xi)$ and $\tilde{P}(\chi_\xi)$ (see, for instance, [30]). However, the MIL framework is based on the consideration of the mixture fraction ξ together with the mass fraction Y of a reactive species, oxygen in the present work, and we can reasonably expect the conditional change of the progress variable Y to be larger for nearly stoichiometric conditions than other conditions. As a result, the independence hypothesis cannot be retained any longer for these two variables. On the contrary, based on the sudden-chemistry hypothesis [31], the MIL model introduces a strong but clearly stated functional dependence

between the two variables. The sudden-chemistry hypothesis is briefly illustrated below.

Based on the simplest micromixing closure, i.e., the one given by the IEM (interaction par echange avec la Moyenne) model [32], the Lagrangian evolution of fluid particle issuing from either oxidizer or fuel stream is given by the following set of equations:

$$\frac{\mathrm{d}\xi}{\mathrm{d}t} = \frac{\tilde{\xi} - \xi}{\tau_\xi} \quad \text{and} \quad \frac{\mathrm{d}Y}{\mathrm{d}t} = \frac{\tilde{Y} - Y}{\tau_Y} + \omega_Y \tag{1}$$

where τ_ξ and τ_Y are the characteristic mixing time scales of the mixture fraction and the oxygen mass fraction, respectively. Within the MIL framework, it is assumed that the chemical reactions are sudden: particles need a finite time to ignite during their evolution toward the mean composition but then instantaneously jump from the IEM mixing line to the equilibrium line. Their trajectory can be drawn in the composition space for fixed values of the mean composition and mixing frequency, as sketched in Fig. 1. It is denoted as $Y^{\mathrm{MIL}}(\xi)$ in the following and it allows expressing the joint scalar PDF as $\tilde{P}(\xi, Y) = \tilde{P}(\xi)\delta(Y - Y^{\mathrm{MIL}}(\xi))$, where $\delta(Y - Y^*)$ denotes the Dirac delta function positioned at $Y = Y^*$.

The corresponding path line $Y^{\mathrm{MIL}}(\xi)$ is fully determined through the knowledge of the mixture fraction values that correspond to the jump positions ξ_{J-} and ξ_{J+}. They are easily obtained by a direct comparison between the mixing time scale and tabulated chemical time scales τ_{chem} that can incorporate the details of the chemical kinetics. For instance, the numerical simulations reported in [33] have been conducted with a tabulated chemical-time-scale library obtained from GRI-Mech [34], which includes 325 elementary steps and 53 species. Previous applications of the model relying on the use of representative chemical kinetics schemes can be also found in [14,31,35]. In the present study, the chemical time scales have been obtained using the chemical kinetics description proposed by

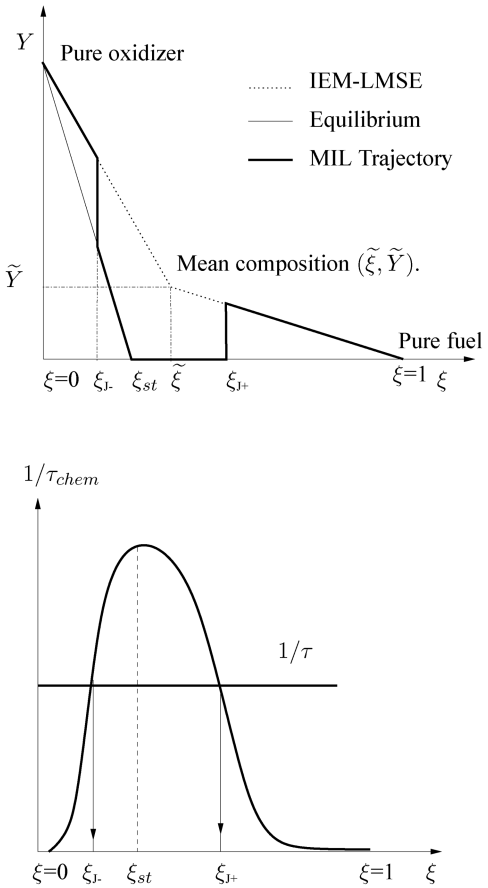

Fig. 1 MIL trajectory (thick lines) in the composition space (ξ, Y). Equilibrium (thin line) and IEM-LMSE (linear mean square estimation) mixing lines (dashed lines) are also depicted.

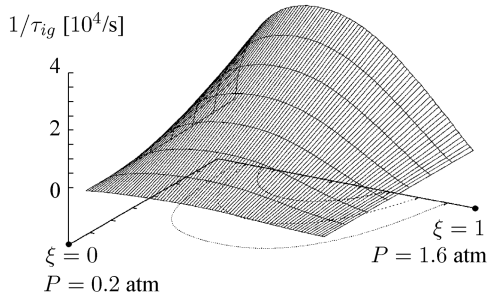

Fig. 2 Representation of the inverse of the self-ignition chemical time scale τ_{ign} as a function of mixture fraction ξ and pressure, the initial temperature level is 1200 K.

Jachimowski [36] that includes 13 species and 33 elementary chemical-reaction steps. The corresponding mechanism has been already used with success to represent supersonic combustion in nonpremixed turbulent coflowing jets. By comparing the resulting chemical time scales with flow time scales, the MIL framework allows delineating an inflammable domain in the mixture fraction space, and this feature makes it well suited to describe the effects associated with finite rate chemistry and/or ignition. Because of the consideration of the corresponding Lagrangian trajectory $Y^{\mathrm{MIL}}(\xi)$, a wide range of combustion regimes can be handled, from the infinitively fast chemistry to complete extinction [33].

In addition, following the early work of Luo and Bray [37], who suggested that such a classical conserved scalar presumed PDF method can be modified to deal with high-speed combustion by replacing the static enthalpy with the stagnation enthalpy, the model has been recently extended to supersonic combustion [14]. The objective with such an extension is to include the ignition phenomena associated with the conversion of kinetic energy into thermal energy via the viscous dissipation heating. This mechanism is likely to affect the early developments of chemical processes and the nonpremixed flame stabilization in high Mach number reactive flows. Indeed, since the chemical source terms are highly temperature-sensitive [27], at high Mach number values, the combustion thermal runaway is strongly influenced by the viscous dissipation phenomena, as reported in the earlier works of Jackson and Hussaini [38], Im et al. [39], and Figueira da Silva et al. [40]. Even if these phenomena do not bring special additional difficulties to simulate laminar reactive flows, the situation is different from the turbulent combustion modeling point of view and some efforts have been already done to take them into account under the fast-chemistry assumption. For instance, a revisited flamelet model has been put forward for nonpremixed combustion in nearly-constant-pressure supersonic turbulent reactive flows by Sabel'nikov et al. [41]. Such a flamelet approach is well suited for sufficiently fast chemistry, whereas the model MIL recently revisited in [14] is able to describe combustion in high-speed flows in situations in which finite rate chemistry effects come into play. We now briefly recall the main features of the closure proposed in [14]. They are as follows:

1) Approximate the Lagrangian evolution of the total enthalpy $h_t(\xi)$ by the IEM trajectory consistently with Eq. (1): i.e., through $\mathrm{d}h_t/\mathrm{d}t = (\tilde{h}_t - h_t)/\tau_\xi$.

2) Deduce from the levels of both the static enthalpy $h(\xi) \approx h_t(\xi) - \tilde{u}_\alpha \tilde{u}_\alpha$ and the mean static pressure $\bar{p}$ the value of an autoignition time scale $\tau_{\mathrm{ig}}(\xi)$ for each value of the mixture fraction ξ (see Fig. 2).

3) This self-ignition time-scale value is compared to an approximated value of the particle age (corresponding to the time elapsed since the particle left either the pure oxidizer or pure fuel injection stream) and this allows delineating a possible domain of spontaneous ignition in the mixture fraction space. Such a direct comparison between the particle age and tabulated chemical induction time takes into account the added functional dependence to velocity through the estimation of static enthalpy $h(\xi)$ from the total enthalpy $h_t(\xi)$. Such an extension has been found to be able to represent self-ignition phenomena that can result from viscous dissipation effects in supersonic mixing layers (see [14]).

Because of the sudden-chemistry assumption that relates the progress variable Y to the mixture fraction field ξ through $Y = Y^{\mathrm{MIL}}(\xi)$, the estimation of the joint scalar PDF $\tilde{P}(Y, \xi; \boldsymbol{x}, t)$ can be simply expressed from the single marginal PDF of the mixture fraction $\tilde{P}(\xi; \boldsymbol{x}, t)$, which is presumed to be a classical beta function PDF. The estimation of the presumed beta PDF for the mixture fraction can be performed through the single knowledge of $\tilde{\xi}$ and $\widetilde{\xi''^2}$. These quantities are calculated through the numerical solution of the following set of transport equations:

$$\frac{\partial \bar{\rho}\tilde{\xi}}{\partial t} + \frac{\partial}{\partial x_k}\left(\bar{\rho}\tilde{u}_k\tilde{\xi} - \bar{\rho}\frac{\nu_T}{Sc_{\tilde{\xi}}}\frac{\partial \tilde{\xi}}{\partial x_k}\right) = 0 \tag{2}$$

$$\frac{\partial \bar{\rho}\widetilde{\xi''^2}}{\partial t} + \frac{\partial}{\partial x_k}\left(\bar{\rho}\tilde{u}_k\widetilde{\xi''^2} - \bar{\rho}\frac{\nu_T}{\underset{\sim}{Sc}_{\widetilde{\xi''^2}}}\frac{\partial \widetilde{\xi''^2}}{\partial x_k}\right) = 2\bar{\rho}\frac{\nu_T}{Sc_{\tilde{\xi}}}\frac{\partial \tilde{\xi}}{\partial x_k}\frac{\partial \tilde{\xi}}{\partial x_k} - \bar{\rho}\frac{\widetilde{\xi''^2}}{\tau_\xi} \tag{3}$$

where molecular diffusion terms are neglected with respect to their turbulent counterparts. In the previous equations, the corresponding turbulent scalar transport terms are closed by using the turbulent eddy viscosity $\nu_T = C_\mu k^2/\epsilon$, with $C_\mu = 0.09$, and the turbulent Schmidt numbers $Sc_{\tilde{\xi}}$ and $Sc_{\widetilde{\xi''^2}}$ are set to their usual value of 0.7 [42]. The mean dissipation rate of the scalar variance is modeled with a standard linear relaxation law based on the dissipation time scale τ_ξ. This quantity, as well as its counterpart for the reactive scalar τ_Y [see Eq. (1)], can be evaluated either due to an algebraic relationship based on the integral turbulent time scale $\tau_T = k/\epsilon$, or through the resolution of a modeled transport equation for the mean scalar dissipation rate as the one proposed by Jones and Musonge [43]. Nevertheless, it should be recognized that the closure of such a transport equation still suffers from certain uncertainties and further work is also needed in this direction, especially when reactive scalars are involved (see, for instance, Mura and Borghi [44] or Mura et al. [45]). In the following, we will suppose that $\tau_\xi = \tau_Y = \tau$. Then the mixing time scale τ is obtained by invoking the usual algebraic closure that assumes it to be proportional to the integral turbulence time τ: i.e., $\tau = C\tau_T$, where C is a modeling constant. It is clear that the validity of this widely used hypothesis depends on the way velocity and scalar fluctuations have been generated. It is equivalent to close the mean scalar dissipation rate by $\tilde{\chi}_\xi = \widetilde{\xi''^2}/(C\tau_T)$, and this supposes the scalar spectrum being fully developed and the rate of scalar mixing being controlled by the rate of scalar variance production at large scales (i.e., a cascade process in equilibrium). Previous studies have revealed that the value of C is influenced by the initial scalar-to-velocity length-scale ratio, but in the absence of any further convincing information about this dependency, we retained the value C equals to unity in such a manner that $\tau = \tau_T = k/\epsilon$ with k the turbulence kinetic energy and ϵ its dissipation rate.

In the present study, the standard k-ϵ approach is retained to model the turbulence. To account for compressibility effects, the pressure dilatation term that appears in the turbulent kinetic energy transport equation is closed as a function of Mt, the turbulent Mach number based on the turbulent kinetic energy, following the strategy introduced by Zeman [46]. The dissipation rate of the turbulent kinetic energy ϵ is modeled as the sum of two contributions. The first one is the classical solenoidal contribution ϵ_s, which is considered to be unaffected by compressible effects: a classical modeled balance equation is retained for this term. The second term is associated with the compressible or dilatational dissipation rate ϵ_c. Following the closure proposal of Zeman [46], it is also a function of the turbulent Mach number Mt.

From this closure, the estimation of the presumed beta PDF for the mixture fraction $\tilde{P}(\xi)$ can then be performed through the knowledge of $\tilde{\xi}$ and $\widetilde{\xi''^2}$ as obtained from Eqs. (2) and (3) at each point of the computational mesh using the standard algorithms from the Numerical Recipes Library [47]. In addition, provided that the MIL trajectory is known (namely, that the mean values $\tilde{\xi}$ and $\tilde{Y}$ and the mixing time scale τ have been evaluated), the mean chemical rate $\overline{\rho\omega_Y}$ is then easily expressed using the PDF of the mixture fraction. The resulting value is finally used as an input to solve the transport equation for the mean species mass fraction $\tilde{Y}$ [14,33].

III. Numerical Solution of the Navier–Stokes Equations

A. Discretization Technique and Resolution Scheme

The computational model described in the previous section has been implemented into the CFD (computational fluid dynamics) code N3SNatur [48]; the numerical strategy on which the code relies is first briefly presented. N3SNatur solves the three-dimensional compressible and reactive Navier–Stokes equations. (In the following, only two-dimensional numerical simulation results are presented.) It is based on a mixed finite volume (FV) and finite element (FE) approach combined with the use of common upwinding algorithms applied on unstructured meshes made up of either triangular elements for two-dimensional numerical simulations or tetrahedral elements for three-dimensional numerical simulations. The discrete form of the complete set of conservative equations is based on both the FE and the FV formulations. Temporal and convective contributions are processed using the FV formulation, whereas viscous and source terms are evaluated using the FE formulation, which is also subsequently used for the total-variation-diminishing (TVD) extension to the second-order precision. In the Cartesian coordinates, the conservative form of the Navier–Stokes equations is considered to describe the temporal and spatial evolution of the vector of conservative variables $\boldsymbol{\mathcal{U}}$. This solution vector $\boldsymbol{\mathcal{U}}$ includes, in a conservative form, mean density $\bar{\rho}$, mean momentum $\overline{\rho u_k}$, mean energy $\overline{\rho E}$, turbulence kinetic energy $\overline{\rho k}$ and its dissipation rate $\overline{\rho\epsilon}$, mean species mass fraction $\overline{\rho Y_i}$, and mixture fraction mean $\overline{\rho\xi}$ and variance $\overline{\rho\xi''^2}$. If we denote Ω as the two-dimensional physical domain under consideration, which is discretized using triangular elements, and ϕ as a test function, the classical variational formulation of the Navier–Stokes equations becomes

$$\frac{\mathrm{d}}{\mathrm{d}t}\int_\Omega \boldsymbol{\mathcal{U}}\phi\,\mathrm{d}V + \int_\Omega \nabla.\boldsymbol{\mathcal{F}}(\boldsymbol{\mathcal{U}})\phi\,\mathrm{d}V = \int_\Omega \nabla.\boldsymbol{\mathcal{D}}(\boldsymbol{\mathcal{U}})\phi\,\mathrm{d}V + \int_\Omega \boldsymbol{\mathcal{S}}\phi\,\mathrm{d}V \tag{4}$$

where $\boldsymbol{\mathcal{F}}$ and $\boldsymbol{\mathcal{D}}$ represent the convective and diffusive fluxes vectors, respectively, and $\boldsymbol{\mathcal{S}}$ stands for the source terms vector. At a given time t, the solution $\boldsymbol{\mathcal{U}}$ can be sought as a piecewise-constant function $\boldsymbol{\mathcal{U}}_h(\boldsymbol{x})$, on the n_C control volumes C_i (FV formulation):

$$\boldsymbol{\mathcal{U}}_h(\boldsymbol{x}) = \sum_{i=1}^{n_C} \boldsymbol{\mathcal{U}}_i\phi_i(\boldsymbol{x}) \tag{5}$$

The test functions ϕ_i are naturally chosen as characteristic functions of the control volume:

$$\begin{cases} \phi_i(\boldsymbol{x}) = 1 & \text{if } \boldsymbol{x} \in C_i \\ \phi_i(\boldsymbol{x}) = 0 & \text{if } \boldsymbol{x} \notin C_i \end{cases} \tag{6}$$

In fact, the same solution can also be sought as a piecewise-linear function on the n_T triangles (FE formulation):

$$\boldsymbol{\mathcal{V}}_h(\boldsymbol{x}) = \sum_{k=1}^{n_T} \boldsymbol{N}_k(\boldsymbol{x})\psi_k(\boldsymbol{x}) \tag{7}$$

where $\psi_k(\boldsymbol{x})$ is the characteristic function for the triangle k and $\boldsymbol{N}_k$ is the interpolation function on each triangle. The equivalence of the two formulations imposes that the constant value $\boldsymbol{\mathcal{U}}_i$ of the FV approximation $\boldsymbol{\mathcal{U}}_h$ in the volume C_i around the node i must be equal to the integrated mean value of the FE formulation $\boldsymbol{\mathcal{V}}_h$ on each finite element intersecting C_i:

$$\int_{C_i} \mathcal{U}_i \, \mathrm{d}V = \sum_k \int_{C_i} \mathcal{V}_h \, \mathrm{d}V \tag{8}$$

Using the Gauss theorem to express the integrals of convective fluxes and the Green identity for the diffusive fluxes, the mixed formulation can be written for each control volume C_i:

$$\frac{\mathrm{d}}{\mathrm{d}t}\int_{C_i} \mathcal{U}_h \, \mathrm{d}V + \int_{\Gamma_i} \boldsymbol{F}(\mathcal{U}_h).\boldsymbol{n}_i \, \mathrm{d}S = -\int_{C_i} \mathcal{D}(\mathcal{V}_h)\nabla \boldsymbol{N}_i \, \mathrm{d}S + \int_{C_i} \mathcal{S}(\mathcal{V}_h)\boldsymbol{N}_i \, \mathrm{d}V \tag{9}$$

where $\boldsymbol{n}_i$ is the normal to the boundary Γ_i of the control cell C_i.

The use of the MUSCL method yields monotonic solutions with a second-order precision in space via variable extrapolation, and the use of flux-limiter functions gives the numerical scheme the TVD property and avoids the merging of spurious numerical oscillations in the vicinity of discontinuities. It is worth mentioning that the limiting function of Van Albada et al. [49] has been retained in the present study. An implicit Euler scheme is retained to perform the temporal integration of all the operators (convective, diffusive, and source terms) of the discretized Navier–Stokes equations. The use of such an implicit discretization scheme leads to a large system of linear algebraic equations that must be solved at each time step. The solution is obtained using a Gauss–Seidel algorithm. The resort to a standard first-order implicit Euler scheme for temporal integration can be justified by the fact that within the framework of the RANS simulation retained in the present study, we are not interested in the details of the transitional behavior of the numerical solution. Only the final converged solutions will be considered and analyzed below.

The transport equations for mean density, momentum, total energy, species, and mixture fraction mean and variance, as given by Eqs. (2) and (3), are solved. The last two quantities allow the estimate of the beta PDF at each point of the computational grid. It is worth noting that considering the MIL skeleton in the composition space, which is made up of piecewise relationships between Y and ξ, all the integral terms that require evaluation after the weighting by the mixture fraction PDF $\tilde{P}(\xi)$ can be expressed as functions of the following two integral forms:

$$\mathcal{A} = \int_a^b \tilde{P}(\xi).\mathrm{d}\xi \quad \text{and} \quad \mathcal{B} = \int_a^b \xi.\tilde{P}(\xi).\mathrm{d}\xi$$

These two integral forms are directly available from the Numerical Recipes Library [47] as polynomial expressions depending on the PDF shape through $\tilde{\xi}$ and $\widetilde{\xi''^2}$ and on the values a and b that bound the domain of integration. This avoids any resort to computational demanding numerical integrations in order to determine the mean chemical rate $\overline{\rho\omega_Y}$ from its instantaneous expression as given in [33].

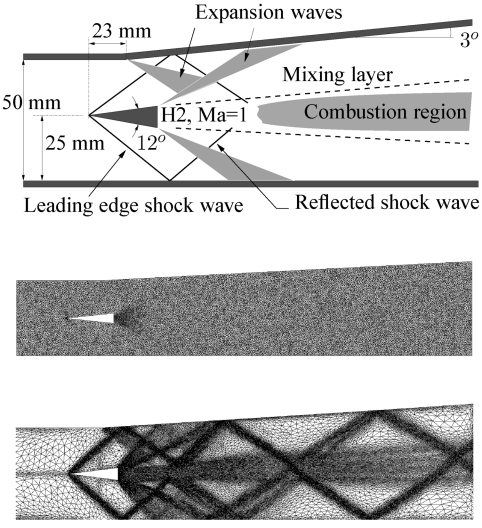

Fig. 3 Sketch of the scramjet combustion model (top); initial (38,000 cells) (middle) and final mesh (45,000 cells) (bottom) retained for the nonreactive simulation after application of the AMA procedure.

B. Mesh Adaptation Strategy

Considering either nonreactive or reactive situations, shock-capturing schemes are all the more efficient that they are combined with a relevant mesh adaptation strategy [50], and the interest and performances associated with classical remeshing techniques have been already nicely illustrated for both nonreactive and reactive situations in many previous studies (see, for instance, [50]). In the present work, the numerical tool ANGENER (anisotropic mesh adaptation generator) developed by Dolejsi [51,52] has been coupled with the N3SNatur CFD solver.

First, an initial triangulation of the computational domain with embedded interior boundaries (associated with the wedge injector) is accomplished by using an automatic mesh generator scheme [53] (see Fig. 3). Then the AMA method on which ANGENER relies is applied to a converged solution obtained on the initial homogeneous mesh (see Fig. 3). The principles of the AMA method differ from conventional adaptive mesh refinement methodologies (see [51,52]). It consists of generating an appropriate new metric space in order to evaluate the lengths of the segments, by weighting these as a function of the local curvature level of the appropriate scalar field chosen (the density in the present case). Then based on the targeted number of elements for the new mesh, a reference length minimizing the interpolation error is determined. A given set of basic local operations are iteratively applied on the edges to obtain a more isotropic distribution of the interpolation error. Compressible structures such as shock and expansion waves can be identified and located, due to the important variations of density in the physical space. The corresponding local curvature level is important in the region of discontinuities, and this yields an interpolation error on unadapted meshes. In the physical space, this strategy does not only consist of inserting or removing nodes in high gradients or low varying zones, respectively, but it also yields a better alignment of the control volumes along the various discontinuities, and so the fluxes are more correctly evaluated in the direction of the propagation of the physical waves [54] since the triangular elements that constitute the new mesh are stretched normal to the isolines of the greatest values of curvature. The corresponding stretching of the control volumes can be monitored by limiting the maximum angle between two edges. Together with an improved numerical accuracy, the insertion (respectively, removal) of nodes in high (respectively, low) scalar-field curvature zones guarantees a similar or even reduced computational cost.

A typical mesh obtained due to this remeshing procedure is reported in Fig. 3. This mesh has been computed from the density field resulting from a nonreactive numerical simulation. The choice of the density field as an indicator to apply the remeshing technique does not only lead to a mesh refinement at the discontinuity locations but also improves the description of the mixing layer between hydrogen and vitiated air that exhibits a large density ratio: namely, $\rho_{\mathrm{air}}/\rho_{\mathrm{H_2}} \approx 10$.

IV. Application to a Scramjet Model

Waidmann et al. [19,20] have gathered a well-documented experimental database on a scramjet combustor model that has been used for several previous numerical investigations [21,23,24]. The test-case geometry is briefly presented below. Then the computational domain and boundary conditions retained to perform the numerical simulations are introduced. Finally, the results of both the nonreactive and reactive simulations are discussed in the light of experimental data.

A. Presentation of the Test Case

A schematic representation of the combustion chamber is reported in Fig. 3. The combustor is 4 cm wide and 5 cm high at the entrance, with a divergent angle of 3 deg of the chamber upper wall. The main

stream consists of preheated air expanded through a Laval nozzle and injected at a Mach number of 2. Downstream of this nozzle, hydrogen is sonically injected through a wedge injector. Along the first 10 cm behind the injector exit the walls are equipped with large optical access windows. Several optical techniques have been used to visualize and characterize the supersonic reactive flowfield. Schlieren, shadowgraphs, Rayleigh scattering, spontaneous OH emission, laser-excited OH fluorescence, particle image velocimetry, and laser Doppler velocimetry (LDV) were applied to gather information about mixing and combustion process in the supersonic airstream [19,20].

The computational simulations reported below are two-dimensional, although the experimental configuration is inherently three-dimensional with 15 circular hydrogen injectors, having a diameter of 1 mm, placed at the base of the wedge-shaped flameholder. The distance between two consecutive holes is 2.4 mm, and the resulting effect of jets interaction will not be considered in the present computations. In the numerical simulations reported below, hydrogen is sonically injected, but through a slot injector (having the same jet area) instead of circular injectors. Since the growth rate of a slot jet differs from the one of round jets, some discrepancies between numerical computations and experimental results could be expected in the near field. In fact, the two-dimensional representation adopted here may certainly be questioned, but we will see that the present numerical simulations lead to a fairly satisfactory prediction of the essential features of the nonreactive flowfield, and with a computational cost significantly lower than that of the corresponding three-dimensional simulations. This confirms the conclusions of the early numerical studies of the scramjet combustor model conducted in [21–23], which were also based on such a two-dimensional simplification.

The boundary conditions used for the present simulations are summarized in Table 1 and Fig. 3; supersonic inlet conditions are used for both air and hydrogen inlets; static pressure, temperature, velocity, and turbulence variables (namely, turbulent kinetic energy k and its dissipation rate ϵ) are set as Dirichlet values. The outlet of the computational domain is set by a compatibility boundary condition, and so only the value of the static pressure is provided. Finally, the inner walls are modeled with a slip condition.

Experiments have shown that a complex system of successive shock wave reflections and expansion waves establishes in the combustion chamber, thus emphasizing that a particular effort is required to represent the strong discontinuities that appear in the flowfield.

B. Nonreactive Simulation

In such a geometry in which hydrogen is directly injected into a high Mach number airstream, the interaction between shock waves and the central jet of hydrogen is of key importance. Previous investigations of such interactions have confirmed the enhancement of the mixing and the stability limits of supersonic jet flames (see, for instance, Huh and Driscoll [9]). Its influence on flame-holding downstream of a strut has been also investigated by, among others, Fujimori et al. [8]. As a result, its accurate representation is expected to be one of the essential ingredients to obtain a realistic description of the flame, and the AMA strategy used here is expected to bring a significant contribution to the achievement of this task. In this respect, the numerical temperature field reported in Fig. 4 rather well illustrates the ability of the method to capture sharp discontinuities.

In a first step of the validation procedure, the qualitative comparison between the numerical isopressure levels obtained in nonreactive conditions and the experimental shadowgraph reported in Fig. 5 confirms that the present numerical strategy leads to a satisfactory description of the essential physical phenomena. Numerical results are in a good qualitative agreement with the flow patterns, as evidenced by the experimental shadowgraphy. Since the diverging section of the experimental setup is only on the upper inner wall, the resulting multiple shock wave reflections give rise to an asymmetrical nonreactive flowfield.

Table 1 Boundary conditions retained for the numerical simulation of the scramjet combustor [19–21]

	Inlet 1	Inlet 2
Ma	2	1
$\tilde{u}$, m/s	730	1200
$\tilde{T}$, K	340	250
$\tilde{p}$, 10^5 Pa	1	1
$\tilde{Y}_{O_2}$	0.232	0
$\tilde{Y}_{H_2O}$	0.032	0
$\tilde{Y}_{H_2}$	0	1
k, m^2/s^2	10	2400
ϵ, m^2/s^3	650	10^8

The corresponding flowfield is complex: a leading-edge oblique shock wave originates at the tip of the injector wedge and is reflected through the whole channel. One can note that an expansion wave is generated on the upper chamber wall, where the divergence starts. Two expansion fans establish on both the lower and upper edges of the injector strut and are followed by recompression shocks. The leading edge and recompression shock waves are reflected through the scramjet chamber and interact with both the shear and mixing layer that develop downstream of the strut.

As shown by Figs. 5–8, the experimental trends are well predicted by the numerical simulation:

1) Discontinuities are well captured and their positioning is computed in a satisfactory way. The shock-induced temperature increase can reach approximately 80 K, as can be seen in Fig. 4. That corresponds to an increase of around 25% with respect to the vitiated air inlet temperature.

2) The underexpanded jet of hydrogen is also well represented (see Figs. 5 and 6). It is worth noting that the hydrogen jet first becomes subsonic after it discharges into the combustion chamber, where it is accelerated by the airstream to reach eventually supersonic conditions downstream of the wedge injector.

3) Minimum and maximum pressure evolutions are qualitatively recovered and velocity cross-stream profiles are in good agreement

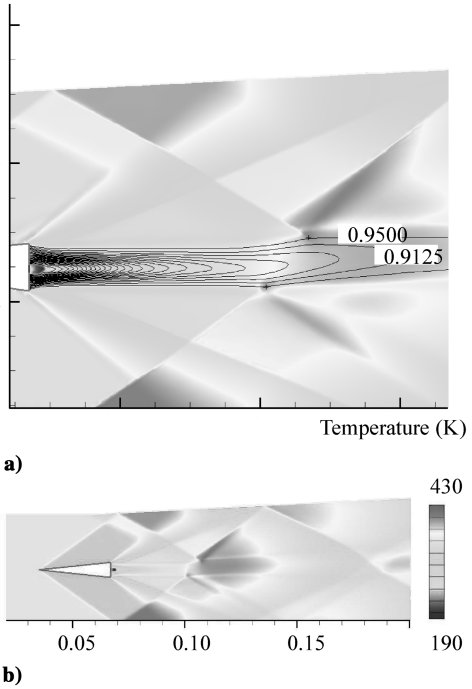

Fig. 4 Mean temperature field as obtained from the nonreactive simulation a) zoom downstream of the injector exit with contour lines of the mean oxygen mass fraction and b) general view of the computational domain.

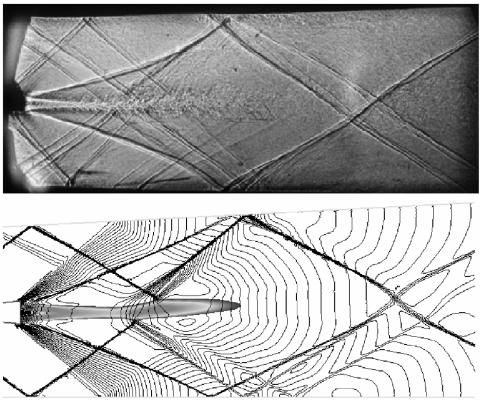

Fig. 5 Shadowgraphy imaging of the nonreactive flowfield (top) and computational pressure contour plots (bottom). The shaded zone downstream of the wedge injector delineates the subsonic jet flow.

with experimental data, despite a little shift toward the upper wall (see Fig. 7). It is noteworthy that such a shift has been also observed in the numerical simulation conducted by Oevermann [21].

4) Cross-stream distributions of the velocity fluctuations $u' = \sqrt{2k/3}$ are shown in Fig. 8. From a qualitative point of view, experimental trends are well recovered with a maximum at the center of the channel. In the upper part of the channel featuring the divergent wall, the turbulence levels are higher than in the lower part of the channel. From a more quantitative point of view, discrepancies can reach 40% with respect to the experimental values. However, experimental data are only available rather far downstream of the injector ($x = 182$ and 207 mm) in a region where the flowfield is strongly perturbed by shock waves reflections (see Fig. 5) and does not facilitate quantitative measurements. As shown later, such important discrepancies are not observed in the reactive simulations, in which more data have been collected in the near ($x = 78$ mm), intermediate ($x = 125$ mm) and far field ($x = 157$ mm) from the hydrogen injector exit.

It should be kept in mind that no special boundary-layer law has been considered to improve the description of the shock wave reflection at the walls, and therefore no special treatment has been included to take either boundary-layer compressions or shock-wave/

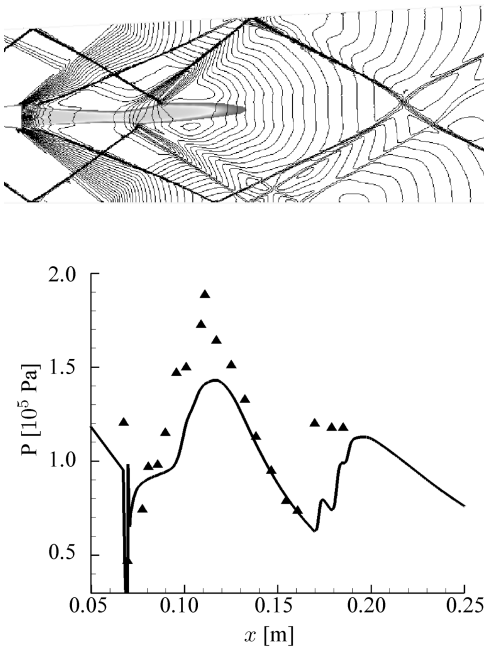

Fig. 6 Isolines of pressure (top) (shaded area delineates the subsonic jet flow) and pressure distribution along the centerline of the channel ($y = 25$ mm) (bottom); experiments (symbols).

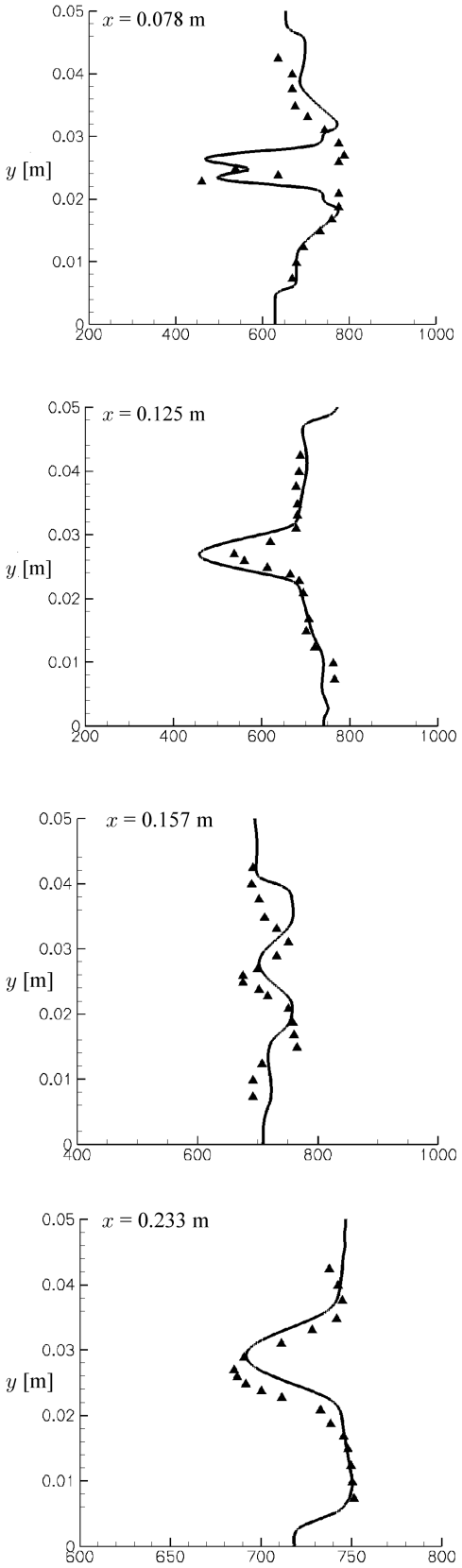

Fig. 7 Axial velocity profiles at four different locations downstream of the wedge injector; numerical simulation (solid lines) and experiments (symbols).

boundary-layer interactions. As shown by Fig. 5, the comparison between computational results and experiments does not appear to be too sensitive to these approximations, which could have led to a significant shift of the successive reflections.

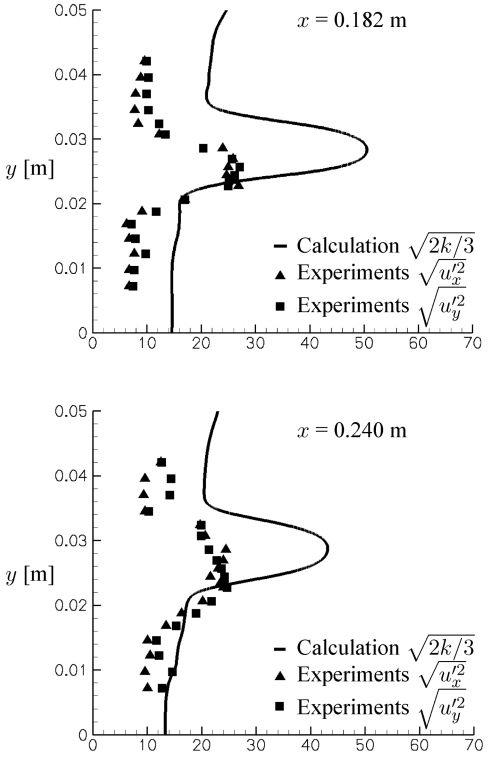

Fig. 8 Cross-stream velocity fluctuation profiles at two different locations; experiments (symbols).

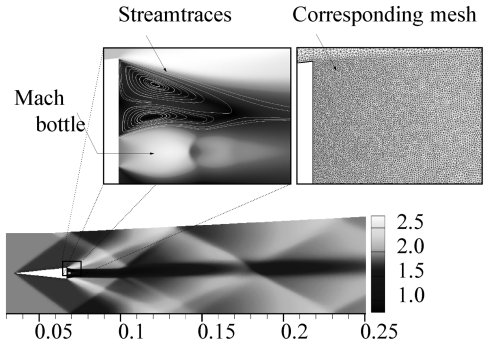

Fig. 9 Mach number field and recirculation zones behind the strut; corresponding refined mesh is also reported.

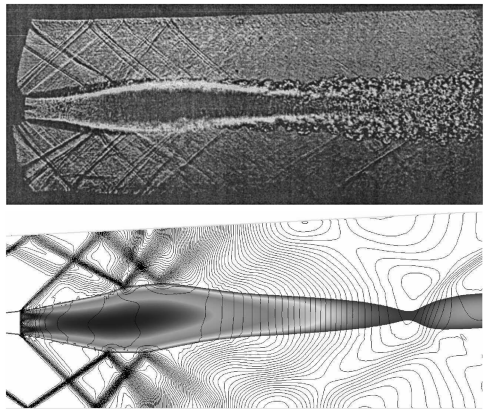

Fig. 10 Shadowgraphy imaging of the reactive flowfield (top) and computational pressure contour plots (bottom). The shaded zone delineates the subsonic jet flow.

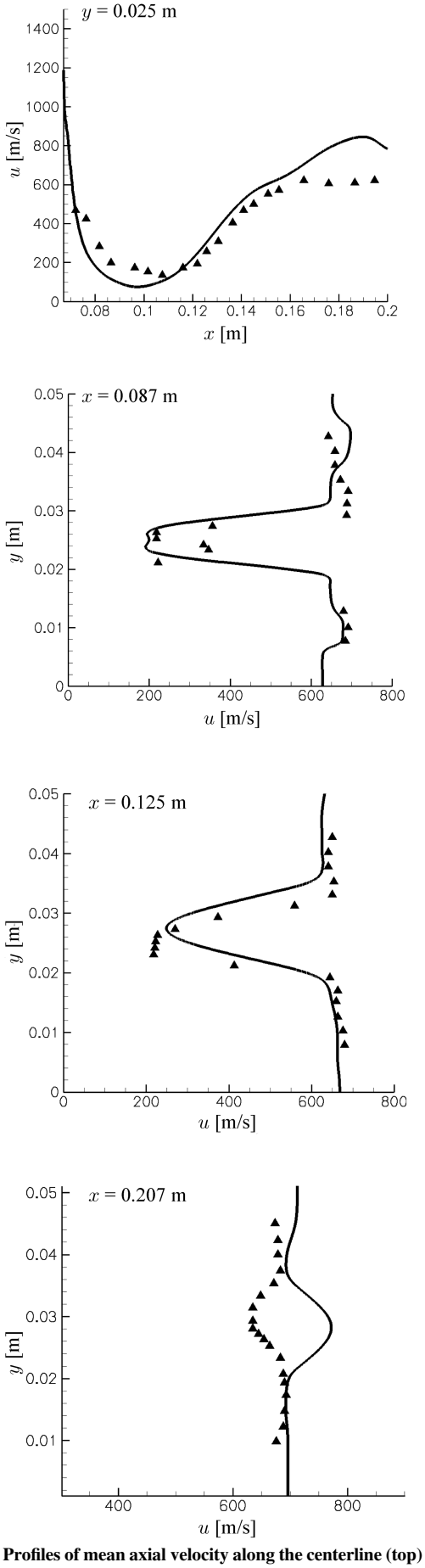

Fig. 11 Profiles of mean axial velocity along the centerline (top) and at different locations downstream of the injector wedge; experiments (symbols).

To conclude this analysis, one should remember that the quantitative analysis of the results requires being cautious, considering the difficulty raised by the difference existing between Reynolds-averaged experimental data and Favre-averaged computational results. This difference increases not only with the Mach number but also with the chemical heat release when turbulent reactive flows, such as those considered in the next section, are concerned.

C. Reactive Simulation

The experimental investigations reported by Waidmann et al. [19,20] mention that in the range of conditions considered, no self-ignition is observed, and so an external source of energy is required to obtain ignition. Indeed, the values of total temperature in the two inlet streams given in Table 1 are not high enough to yield sufficiently small values of the ignition delays. Nevertheless, in scramjet combustion chambers, the wedge injector itself also acts as a flameholder. Figure 9 provides a detailed view of the wake region downstream of the injector. In this figure, the Mach number field obtained from the nonreactive simulation is plotted together with stream traces displaying two pairs of counter-rotating vortices.

From the numerical point of view, once the solution of the nonreactive simulation is converged, we use an ignition method that consists of filling a square zone in the wake of the hydrogen injector with fully burned gases. The ignition process is only applied at the first step of the computation, once the solution of the corresponding nonreactive simulation is converged. Subsequently, the flame stabilization results only from the MIL model of turbulent combustion. Remeshing steps are then performed by following the methodology described by Lehnasch and Bruel [54], and only the final results are reported in the present section.

The global structure of the flowfield in the presence of chemical reactions is reported in Fig. 10. The computational pressure contour evidences the reflected shock wave locations that determine the position of the maximum width of the reaction zone, which appears to be entirely subsonic. It is delineated by the shaded area in Fig. 10. Previous studies have stressed the important role played by such shock waves interactions on both mixing efficiency and flame stabilization processes [8,9]. Fujimori et al. [8] have evidenced that incident shock waves significantly affect the sizes and locations of the recirculation zone and thus increase the role of these recirculation zones as flame holders. The dimensions of the subsonic reaction zone seems to be a little bit overestimated with respect to the experimental results, but the agreement obtained on the velocity profiles is satisfactory (see Fig. 12). Figure 11 (top) displays the mean axial velocity profile along the line $y = 25$ mm. A region of strong deceleration directly follows the injection of hydrogen. Then the stream is accelerated to reach values close to sonic conditions at $x = 180$ mm, where a weak compression wave crosses the centerline. The maximum value of velocity is overestimated, but in comparison with previous numerical simulations results [21], no shock wave formation is observed at this special location. This behavior is in better agreement with the experimental data [19,20] than with previously reported results.

The temperature field and the cross-stream profiles of temperature at different locations downstream of the injector wedge are given in Fig. 12. Computational results show a fairly good agreement in terms of temperature levels with the experimental data. Furthermore, the only noticeable discrepancies are likely to result from the aerodynamical description itself and not from the combustion model.

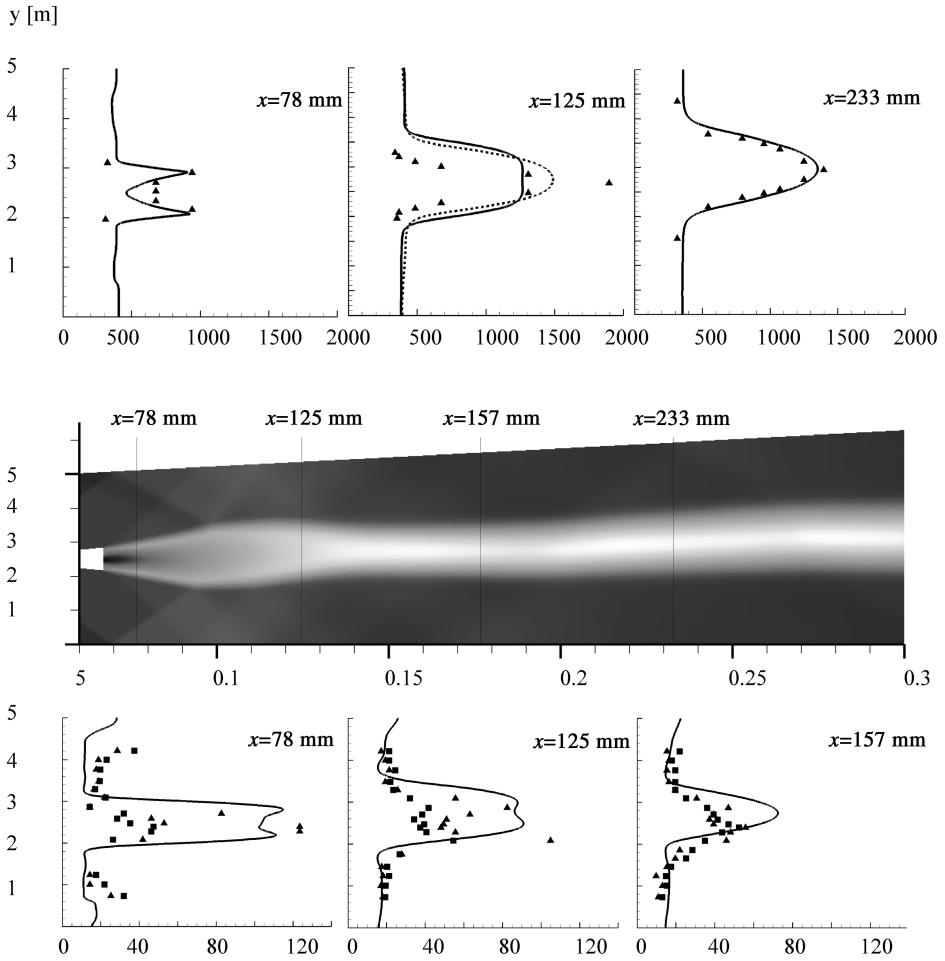

Fig. 12 Mean temperature cross-stream profiles at different locations (top); associated mean temperature field (middle), and velocity fluctuations cross-stream velocity fluctuation profiles at different locations downstream of the injector wedge (bottom); computational results (solid lines), temperature profile at $x = 140$ mm (dotted line), and experiments (symbols).

Indeed, the description of reflected shock wave positions clearly determines the positions of the minimum and maximum width of the reaction zone. The imperfect representation of the shock wave reflections with inner walls can lead to a certain shift of the location at which it interacts with the reaction zone, thus modifying the dimensions of the subsonic jet flow, as already stressed above. Our computations predict the temperature maximum level at a position $x = 140$ mm, whereas the experimental maximum level is found to be at a position $x = 125$ mm. Despite this small difference, the experimental levels of both temperature and turbulent kinetic energy are rather well recovered at the different positions downstream of the injector.

Cross-stream profiles of velocity fluctuations $u' = \sqrt{2k/3}$ obtained from the simulations together with LDV data of the variance of the velocity components u_x and u_y are displayed in Fig. 12. These results show a satisfactory agreement between the experimental data and the numerical result obtained within the framework of the k-ϵ model, which includes the additional compressible terms of Zeman [46].

V. Conclusions

An efficient RANS—AMA strategy has been used to calculate both nonreactive and reactive turbulent high-speed flows in a laboratory scramjet combustion chamber. The turbulent combustion model is based on a tabulated chemistry and only requires evaluating the mixture fraction PDF, which makes it suitable to predict the essential features of the turbulence chemistry interaction with a minimal amount of computational time. Once applied to the numerical simulation of a scramjet combustor model it is found that despite its simplicity, the approach retained to describe nonpremixed turbulent combustion in high-speed flows is able to recover the main experimental trends. Numerical simulations show a fairly satisfactory agreement with the available experimental data, and the nonpremixed flame structure is well recovered in terms of both its global shape and quantitative measurements obtained at several distinct locations downstream of the injector wedge. Henceforth, the numerical code and modeling strategy are shown to be viable tools for further developments and investigations in the field of supersonic combustion modeling.

Nevertheless, it should be mentioned that further work is now required to improve the representation of the turbulence in such compressible flows. Indeed, a satisfactory aerodynamical description of the turbulent flowfield is a prerequisite to further improve the description of the stabilization of combustion in such complex geometries. In this respect, the use of a refined description of the shock-wave/boundary-layer interaction can play an important role. From the turbulent combustion modeling point of view, further work is also necessary to consider other specific features encountered in supersonic combustion. The issue related to the prediction of the autoignition phenomena that arises from the conversion of kinetic to thermal energy when high-enthalpy streams are considered has been recently addressed [14] and it will be interesting to evaluate the present modeling strategy for the case of a scramjet combustor model featuring such conditions. In this respect, the experiments conducted with a single H_2 fuel injector described in [55] provide useful databases for the purpose of numerical simulation validation. From the modeling point of view, another challenging issue is related to the improvement of the description of turbulent transport, an issue that has received special attention in the early works of Luo [56], but that still remains unanswered by classical RANS or LES computational models.

Acknowledgments

Financial support from Centre National d'Etudes Spatiales and Snecma (Safran Group, Space Engines Division) and from Centre National de la Recherche Scientifique is gratefully acknowledged. The authors have benefited from valuable interactions with Guillaume Lehnasch (LEA, Poitiers, France), François-Xavier Demoulin (Coria, Rouen, France), Luis Fernando Figueira da Silva (PUC, Rio de Janeiro, Brazil), and Vladimir Sabel'nikov (ONERA, France).

References

[1] Timnat, Y. M., "Ramjets and Scramjets," *Advanced Airbreathing Propulsion*, edited by E. F. Strotheer, and D. M. Waltz, Orbit Series Book, Krieger, Malabar, FL, 1996, pp. 7–49.

[2] Ferri, A., (1968) "A Review of Scramjet Propulsion Technology," *Journal of Aircraft*, Vol. 5, No. 1, 1968, pp. 3–10. doi:10.2514/3.43899

[3] Curran, E. T., Heiser, W., and Pratt, D. T., "Fluid Phenomena in Scramjet Combustion Systems," *Annual Review of Fluid Mechanics*, Vol. 28, 1996, pp. 323–360. doi:10.1146/annurev.fl.28.010196.001543

[4] Heiser, W., and Pratt, D. T., *Hypersonic Airbreathing Propulsion*, edited by J. S. Przemieniecki, AIAA Education Series, AIAA, Washington, D.C., 1994.

[5] Bray, K. N. C., Libby, P. A., and Williams, F. A., "High speed turbulent combustion," *Turbulent Reacting Flows*, edited by P. A. Libby, and F. A. Williams, Academic Press, New York, 1994, pp. 609–638.

[6] Bogdanoff, D. W., "Compressibility effects in turbulent shear layers," *AIAA Journal*, Vol. 21, No. 6, 1983, pp. 926–927. doi:10.2514/3.60135

[7] Papamoschou, D., and Roshko, A., "The Compressible Turbulent Shear Layer: An Experimental Study," *Journal of Fluid Mechanics*, Vol. 197, 1988, pp. 453–477. doi:10.1017/S0022112088003325

[8] Fujimori, T., Murayama, M., Sato, J., Kobayashi, H., and Niioka, T., "Flame Holding Behind a Wedge by Incident Shock Waves," *IUTAM Symposium on Combustion in Supersonic Flows*, edited by M. Champion, and B. Deshaies, Kluwer Academic, Norwell, MA, 1997, pp. 95–110.

[9] Huh, H., and Driscoll, J. F., "Shock-Wave-Enhancement of the Mixing and the Stability Limits of Supersonic Hydrogen-Air Jet Flames," *Proceedings of the Combustion Institute*, Vol. 26, 1996, pp. 2933–2939.

[10] Buckmaster, J., Jackson, T. L., and Kumar, A. (eds.), *Combustion in High Speed Flows*, ICASE/LaRC Interdisciplinary Series in Science and Engineering, Kluwer Academic, Norwell, MA, 1994.

[11] Borghi, R., and Pourbaix, E., "On the Coupling of Complex Chemistry with a Turbulent Combustion Model," *Physicochemical Hydrodynamics: PCH*, Vol. 2, 1981, pp. 65–77.

[12] Borghi, R., and Gonzalez, M., "Applications of Lagrangian Models to Turbulent Combustion," *Combustion and Flame*, Vol. 63, 1986, pp. 239–250. doi:10.1016/0010-2180(86)90124-0

[13] Izard, J. F., and Mura, A., "A Lagrangian Model for Nonpremixed Combustion in Supersonic Turbulent Flows," *Proceedings of the 18th International Shock Interaction Symposium*, Centre National de la Recherche Scientifique, Rouen, France, July 2008, pp. 207–212.

[14] Izard, J. F., and Mura, A., "A Lagrangian Model of Combustion in High Speed Flows: Application to Scramjet Conditions," *Combustion Science and Technology*, Vol. 181, No. 11, 2009, pp. 1372–1396. doi:10.1080/00102200903181892

[15] Cheng, T. S., Wehrmeyer, J. A., Pitz, R. W., Jarret, O., and Northam, G. B., "Raman Measurement of Mixing and Finite-Rate Chemistry in a Supersonic Hydrogen-Air Diffusion Flame," *Combustion and Flame*, Vol. 99, 1994, pp. 157–173. doi:10.1016/0010-2180(94)90087-6

[16] Baurle, R. A., Alexopoulos, G. A., and Hassan, H. A., "Modelling of Supersonic Turbulent Combustion Using Assumed Probability Density Functions," *Journal of Propulsion and Power*, Vol. 10, No. 6, 1994, pp. 777–786. doi:10.2514/3.23815

[17] Baurle, R. A., Hsu, A. T., and Hassan, H. A., "Assumed and Evolution Probability Density Functions in Supersonic Turbulent Combustion Calculations," *Journal of Propulsion and Power*, Vol. 11, No. 6, 1995, pp. 1132–1138. doi:10.2514/3.23951

[18] Möbus, H., Gerlinger, P., and Brüggemann, D., "Scalar and Joint Scalar-Velocity-Frequency Monte Carlo PDF Simulation of Supersonic Combustion," *Combustion and Flame*, Vol. 132, Nos. 1–2, 2003, pp. 3–24. doi:10.1016/S0010-2180(02)00428-5

[19] Waidmann, W., Alff, F., Bohm, M., Brummund, U., Clauss, M., and Oschwald, M., "Supersonic Combustion of Hydrogen/Air in a Scramjet Combustion Chamber," *Space Technology*, Vol. 15, No. 6, 1995, pp. 421–429.

doi:10.1016/0892-9270(95)00017-8
[20] Waidmann, W., Brummund, U., and Nuding, J., "Experimental Investigation of Supersonic Ramjet Combustion (Scramjet)," *Transport Phenomena in Combustion*, edited by S. H. Chan, Vol. 2, Taylor and Francis, Washington, D.C., 1995, pp. 1473–1484.
[21] Oevermann, M., "Numerical Investigation of Turbulent Hydrogen Combustion in a Scramjet Using Flamelet Modelling," *Aerospace Science and Technology*, Vol. 4, 2000, pp. 463–480. doi:10.1016/S1270-9638(00)01070-1
[22] Wepler, U., Huhn, Ch., and Koschel, W. W., "Numerical Simulation of Shock Wave Interaction Effects on Supersonic Mixing Layer Growth," *Numerical Flow Simulation II*, Vol. 75, edited by E. H. Hirschel, Notes on Numerical Fluid Mechanics, Springer–Verlag, New York, 2001, pp. 217–228.
[23] Wepler, U., and Koschel, W. W., "Numerical Investigation of Turbulent Reacting Flows in a Scramjet Combustor Model," AIAA Paper 2002-3572, July 2002.
[24] Berglund, M., and Fureby, C., "Les Of Supersonic Combustion in a Scramjet Engine Model," *Proceedings of the Combustion Institute*, Vol. 31, 2007, pp. 2497–2504. doi:10.1016/j.proci.2006.07.074
[25] Génin, F., Chernyavsky, B., and Menon, S., "Large Eddy Simulation of Scramjet Combustion Using a Subgrid Mixing/Combustion Model," AIAA Paper 2003-7035, Dec. 2003.
[26] Bilger, R. W., "Turbulent Jet Diffusion Flames," *Progress in Energy and Combustion Science*, Vol. 1, 1976, pp. 87–109. doi:10.1016/0360-1285(76)90022-8
[27] Williams, F. A., *Combustion Theory*, 2nd ed., Benjamin/Cummins, Menlo Park, CA, 1985.
[28] Borghi, R., "Turbulent Combustion Modelling," *Progress in Energy and Combustion Science*, Vol. 14, 1988, pp. 245–292. doi:10.1016/0360-1285(88)90015-9
[29] Eifler, P., and Kollmann, W., "PDF Prediction of Supersonic Hydrogen Flames," AIAA Paper 93-0448, Jan. 1993.
[30] Peters, N., "Laminar Flamelet Concept in Turbulent Combustion," *Proceedings of the Combustion Institute*, Vol. 21, 1986, pp. 1231–1250.
[31] Obounou, M., Gonzalez, M., and Borghi, R., "A Lagrangian Model for Predicting Turbulent Diffusion Flames with Chemical Kinetic Effects," *Proceedings of the Combustion Institute*, Vol. 25, 1994, pp. 1107–1113.
[32] Villermaux, J., and Devillon, J. C., "Représentation de la Coalescence et de la Redispersion des Domaines de Ségrégation dans un Fluide par un Modèle d'Interaction Phénoménologique," *Proceedings of the 2nd International Symposium on Chemical Reaction Engineering*, Vol. B 1-13, Elsevier, Amsterdam, 1972.
[33] Mura, A., and Demoulin, F. X., "Lagrangian Intermittent Modelling of Turbulent Lifted Flames," *Combustion Theory and Modelling*, Vol. 11, No. 2, 2007, pp. 227–257.
[34] GRI-Mech, Software Package, Ver. 2.11, Gas Research Inst., Chicago, 1997, http://www.ME.Berkeley.edu/gri-mech/ [retrieved 2010].
[35] Fallot, L., Gonzalez, M., Elamraoui, R., and Obounou, M., "Modelling Finite-Rate Chemistry Effects in Nonpremixed Turbulent Combustion: Test on the Bluff-Body Stabilized Flame," *Combustion and Flame*, Vol. 110, 1997, pp. 298–314. doi:10.1016/S0010-2180(97)00077-1
[36] Jachimowski, C. J., "An Analytical Study of the Hydrogen-Air Reaction Mechanism with Application to Scramjet Combustion," NASA TP 2791, 1988.
[37] Luo, K. H., and Bray, K. N. C., "Combustion-Induced Pressure Effects in Supersonic Diffusion Flames," *Proceedings of the Combustion Institute*, Vol. 27, 1998, pp. 2165–2171.
[38] Jackson, T. L., and Hussaini, M. Y., "An Asymptotic Analysis of Supersonic Reacting Mixing Layers," *Combustion Science and Technology*, Vol. 57, 1988, pp. 129–140. doi:10.1080/00102208808923948
[39] Im, H. G., Bechtold, J. K., and Law, C. K., "Analysis of Thermal Ignition in Supersonic Flat Plate Boundary Layers," *Journal of Fluid Mechanics*, Vol. 249, 1993, pp. 99–120. doi:10.1017/S0022112093001090
[40] Figueira da Silva, L. F., Deshaies, B., and Champion, M., "Numerical Study of Ignition Within Hydrogen-Air Supersonic Boundary Layers," *AIAA Journal*, Vol. 31, No. 5, 1993, pp. 884–890. doi:10.2514/3.11700
[41] Sabel'nikov, V. A., Deshaies, B., and Figueira da Silva, L. F., "Revisited Flamelet Model for Nonpremixed Combustion in Supersonic Turbulent Flows," *Combustion and Flame*, Vol. 114, Nos. 3–4, 1998, pp. 577–584.
[42] Launder, B. E., "Heat and Mass Transport," *Turbulence, Topics in Applied Physics*, edited by P. Bradshaw, Springer Verlag, Berlin, 1976, pp. 231–287.
[43] Jones, W. P., and Musonge, P., "Closure of the Reynolds Stress and Scalar Flux Equations," *Physics of Fluids*, Vol. 31, 1988, pp. 3589–3604. doi:10.1063/1.866876
[44] Mura, A., and Borghi, R., "Towards an Extended Scalar Dissipation Equation for Turbulent Premixed Combustion," *Combustion and Flame*, Vol. 133, 2003, pp. 193–196. doi:10.1016/S0010-2180(02)00565-5
[45] Mura, A., Robin, V., and Champion, M., "Modelling of Scalar Dissipation in Partially Premixed Turbulent Flames," *Combustion and Flame*, Vol. 149, Nos. 1–2, 2007, pp. 217–224. doi:10.1016/j.combustflame.2006.11.004
[46] Zeman, O., "Dilatation Dissipation: The Concept and Application in Modelling Compressible Mixing Layers," *Physics of Fluids*, Vol. 2, No. 2, 1990, pp. 176–188.
[47] Press, W. H., Flannery, B. P., Teukolsky, S. A., and Vetterling, W. T., *Numerical Recipes in Fortran 90, The Art of Parallel Scientific Computing*, Cambridge Univ. Press, New York, 1999.
[48] N3SNatur, Software Package, Ver. 1.4, Simulog, Cannes France, 2001.
[49] Van Albada, G. D., Van Leer, B., and Roberts, W. W., "A Comparative Study of Computational Methods in Cosmic Gas Dynamics," *Astronomy and Astrophysics*, Vol. 108, 1982, pp. 76–84.
[50] Figueira da Silva, L. F., Azevedo, J. L. F., and Korzenowski, H., "Unstructured Adaptive Grid Flow Simulations of Inert and Reactive Gas Mixtures," *Journal of Computational Physics*, Vol. 160, No. 2, 2000, pp. 522–540. doi:10.1006/jcph.2000.6470
[51] Dolejsi, V., "Anisotropic Mesh Adaptation for Finite Volume and Finite Element Methods on Triangular Meshes," *Computing and Visualization in Science*, Vol. 1, 1998, pp. 165–178. doi:10.1007/s007910050015
[52] Dolejsi, V., "Anisotropic Mesh Adaptation Technique for Viscous Flow Simulation," *East-West Journal of numerical mathematics*, Vol. 9, No. 1, 2001, pp. 1–24.
[53] Guezaine, C., and Remacle, J. F., "Gmsh: A Three-Dimensional Finite Element Mesh Generator with Built-In Pre- and Post-Processing Facilities," Sept. 2009. http://www.geuz.org/gmsh/ [retrieved 2010].
[54] Lehnasch, G., and Bruel, P., "A Robust Methodology for RANS Simulations of Highly Underexpanded Jets," *International Journal for Numerical Methods in Fluids*, Vol. 56, No. 12, 2008, pp. 2179–2205. doi:10.1002/fld.1613
[55] Cutler, A. D., Danehy, P. M., O'Byrne, S., Rodriguez, C. G., and Drummond, J. P., "Supersonic Combustion Experiments for CFD Model Development and Validation," 42nd AIAA Aerospace Sciences Meeting and Exhibit, AIAA Paper 2004-0266, Jan. 2004.
[56] Luo, K. H., "Combustion Effects on Turbulence in a Partially Premixed Supersonic Diffusion Flame," *Combustion and Flame*, Vol. 119, 1999, pp. 417–435. doi:10.1016/S0010-2180(99)00074-7

J. Oefelein
Associate Editor